Proceedings of the ASME 2010 3rd Joint US-European Fluids Engineering Summer Meeting and 8th International Conference on Nanochannels, Microchannels, and Minichannels
FEDSM-ICNMM2010
August 1-5, 2010, Montreal, Canada

FEDSM-ICNMM2010-31112

AN EXPERIMENTAL STUDY OF A SYNTHETIC JET IN CROSS FLOW IN A MICROCHANNEL

Alexander Sinclair, John Reizes, Victoria Timchenko, and Gary Rosengarten
School of Mechanical and Manufacturing Engineering
University of New South Wales
Sydney, NSW, Australia 2052

ABSTRACT

Laminar flow limits the mixing performance and heat transfer rates that occurs within microdevices. Synthetic jets in the microscale could disrupt laminar flow and improve the performance of such devices. In this paper a synthetic microjet integrated in a microchannel was designed and fabricated using micromachining techniques. The channel flow was driven by a syringe pump at a rate of 1.39μL/s and the device was actuated using a piezoceramic disc at a frequency of 600Hz. Flow fields were measured phase locked to the actuation cycle using the MicroPIV technique in the mid plane of the jet. The resultant fields revealed a jet with a largest velocity of 2.3m/s. The average velocity during expulsion was estimated to be 0.73m/s using a comparison to the oscillatory solution to flow in a square duct. Measurements at different phases in the cycle revealed a jet strong enough to impinge on the opposing wall and the growth and decay of a pair of vortices formed at the edge of the orifice. It was also shown that the synthetic jet significantly altered the flow patterns showing promising signs for enhancing mixing and heat transfer in microchannels.

NOMENCLATURE

d orifice width, m
d_h hydraulic diameter of the orifice, m
D_h hydraulic diameter of the microchannel, m
f actuation frequency, Hz
h etch depth, m
Q flow rate in microchannel, L/s
Re_c Reynolds number of the channel, $\overline{V_c} D_h / \nu$
Re_j Reynolds number of the jet, $\overline{V_j} d_h / \nu$
S Stokes number, $(\omega d_h / \nu)^{1/2}$
T period of actuation cycle, 1/*f*, s
t^* non-dimensional time, *t/T*
$\overline{V}_c$ average velocity in the microchannel, m/s
$\overline{V}_j$ average velocity in the orifice during expulsion, m/s
W channel width, m
x streamwise coordinate in relation to the channel, m
y spanwise coordinate in relation to the channel, m
z depthwise coordinate, m
$2z_{corr}$ depth of correlation, m
μ dynamic viscosity, kg/(m s)
ν kinematic viscosity, m^2/s

INTRODUCTION

A synthetic jet actuator is a device that uses a periodic motion of a diaphragm or a piston inside a cavity to form a jet through an orifice. Synthetic jet actuators transfer momentum to a system but generate zero mass flow through the orifice and thus require no external supply of fluid. Starting with the work of Smith and Glezer [1] over a decade ago, this unique property of synthetic jets has made them a highly attractive device for investigation. The potential applications for such a device include separation control for drag reduction [2], enhanced mixing [3] and thermal management [4].

Advances in micromachining techniques and the creation of the MEMS (Micro-Electro-Mechanical Systems) field have lead

to the development of wide variety of microdevices such as microreactors and biosensors. A key property of such devices is their mixing performance which is critically important in chemical reactions. At this scale Reynolds numbers are low, resulting in laminar flow so that mixing occurs by diffusion only. Synthetic jets have been proposed [5-9] as an active way of disrupting laminar flow and promoting mixing in microchannels. MEMS based synthetic microjet actuators have been developed [8] and received a large amount of attention in numerical studies (e.g. [5-10]). Despite the large number of detailed experimental investigations of macro synthetic jets, due to fabrication and measurement difficulties on the microscale, only a few studies (e.g. [11, 12]) exist on synthetic microjets.

There is a need to fabricate synthetic microjet devices and experimentally examine in detail the velocity fields produced by them. This paper is a report on the construction of a microchannel in which a synthetic jet actuator has been integrated and the PIV measurements of the resulting flow fields.

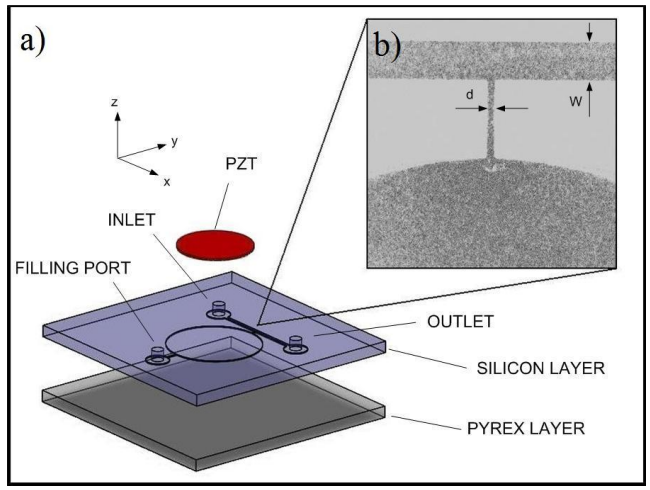

FIGURE 1. (a) Exploded view of experimental device (b) Fluorescent image of the microchannel (grey scales inverted for clarity)

PARAMETERS

Two independent non-dimensional parameters, the Reynolds number, *Re*, and the Stokes number, *S* are commonly used to characterize the fluid flow generated by synthetic jets. The Reynolds number in this work is defined as

$$Re = \frac{\overline{V_j} d_h}{\nu} \tag{1}$$

in which $\overline{V_j}$ is the average velocity over half a cycle at the exit of the orifice, d_h is the hydraulic diameter of the orifice and ν is the kinematic viscosity. The Stokes number is delineated by:

$$S = \sqrt{\frac{2\pi f d_h^2}{\nu}} \tag{2}$$

in which f is the frequency of operation of the actuator.

EXPERIMENTAL SETUP

In this study a microdevice consisting of a synthetic jet actuator integrated in a microchannel was designed and fabricated. The design of the device was based upon the work on micropumps by Morris and Forster [13]. Figure 1 shows an exploded view of the device. The microchannel was 250μm wide with 10mm between inlet and outlet. A large 8mm diameter chamber was connected to the channel by a narrow, 50μm wide and 500μm long slot, called the nozzle. The slot intersected the channel midway along its length forming a T-junction as shown in Figure 1 (b). A third port was incorporated in the design at the back of the chamber to aid in filling. The entire pattern was 72μm deep with near vertical walls. A synthetic jet was generated by the variation in the volume of the chamber resulting from a controlled signal driving a piezoceramic (PZT) disc bonded to the back of the silicon layer.

Fabrication

A 4 inch polished silicon wafer with a thickness of 500μm was used to fabricate the patterned surface described above. One lithography step was required and hence only one mask was needed. The mask design contained a number of different device designs all of which could be fitted onto the one 4 inch wafer. A layer of the photoresist SU-8 was spun onto the wafer and the pattern was exposed and developed. Then, the wafer was etched with an Inductive-Couple-Plasma (ICP) etcher to a depth of 72μm. The etched silicon wafer was split into separate chips using a diamond tipped dicing saw. Inlet/outlet holes were mechanically drilled in the silicon chips using a 1mm diameter diamond tipped drill bit. The etched pattern in the chips was sealed by anodically bonding a 500μm thick Pyrex glass cover.

A 6.4mm diameter circular piezoceramic disc (PSI-5A-4E Piezo Systems Inc) was bonded to the back of the silicon layer using a conductive epoxy. Wires were soldered to the top of the PZT disc and to an area of the conductive epoxy using a solder/flux kit (Piezo Systems Inc).

A schematic diagram of the experimental set up can be seen in Figure 2. A frame manufactured in aluminium held the silicon chip in place and enabled two 1mm inner diameter PEEK tubes (Upchurch Scientific 1538) to be connected to the chip by two nut and ferrule sets (Upchurch Scientific P-225/P-200N). Small lengths of Tygon tubing were connected to the PEEK tubing,

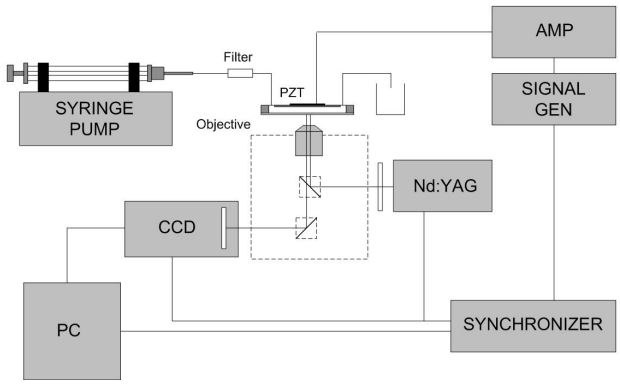

FIGURE 2. Schematic diagram of experimental apparatus

thereby enabling bends to be fitted in the fluid line. A syringe (SGE gastight 5mL) driven by a syringe pump (PHD2000 Harvard apparatus) provided the fluid flow. A 10μm in-line filter was incorporated in the apparatus to prevent blockages of the microchannel by 'large' particles but allowed the much smaller seed particles to pass through. The outlet of the line issued into a small reservoir which was open to the atmosphere. The sinusoidal signal for actuation of the PZT was provided by a signal generator (INSTEK function generator GFG-8216A) and amplified by an amplifier (Derritron Electronic Vibrators Ltd) so as to generate a sufficiently large voltage to drive the PZT disc. The signal generator had a built-in TTL output, which was used as the reference signal for the acquisition of images used in the MicroPIV measurements.

MicroPIV measurements

Velocity measurements were made using the Micro Particle Image Velocimetry (MicroPIV) technique as established by Meinhart et al [14]. Phase averaged velocity field measurements were made using a commercial MicroPIV setup (Lavision Gmbh) on the centre plane of the channel and the orifice perpendicular to the z axis shown in Figure 1. The object plane was imaged using a long working distance objective lens with a magnification M=40 and numerical aperture NA=0.6. A 12-bit, 1376 by 1040 pixel CCD camera (PCO Sensicam QE) recorded the images with a field of view of approximately 222μm x 168μm. In order to capture the full channel width of 250μm, multiple windows were required and stitched together for the final result. Volume illumination of the channel was provided by a 40mJ Nd:YAG laser (Litron Nano S30-15).

De-ionised water was used as the working fluid and seeded with 0.5μm diameter fluorescent particles (Duke Scientific Inc. Ex.Em = 542/612nm). A low seeding concentration of 0.01% by volume was used to ensure good visibility and to minimise particle agglomerations. The setup described provided a measurement thickness known as the depth of correlation $2z_{corr}$ in MicroPiv of 5.5μm using the equation developed by Adrian and Olsen [15].

Images were acquired and processed by the DaVis software package. The actuation cycle was divided into 18 equally spaced segments with 50 image pairs recorded for each. The vector calculation was performed using an iterative cross-correlation method with decreasing window size by a factor of two. A large initial window size of 128 by 128 pixels was employed in order to capture the high velocity regions with a final window of 32 x 32 pixels to provide adequate spatial resolution. The algorithm employed was an averaging algorithm in which the correlation data rather than the velocity measurements were averaged to determine the final averaged velocity vectors for each phase. The initial passes used a second order correlation and the final pass used a standard forward difference scheme. In all passes a window overlap of 50% was used. This provided a final spatial resolution of 2.6μm.

RESULTS AND DISCUSSION

Device Characterisation

The flow rate Q in the microchannel supplied by the syringe pump was set to 1.39μL/s. This resulted in an average velocity $\overline{V}_c$ of 0.077m/s and a Reynolds number, Re_c of 9. Velocity measurements were made on the centre plane of the channel as may be seen in Figure 3, in the vicinity of the orifice. In Figure 3, the

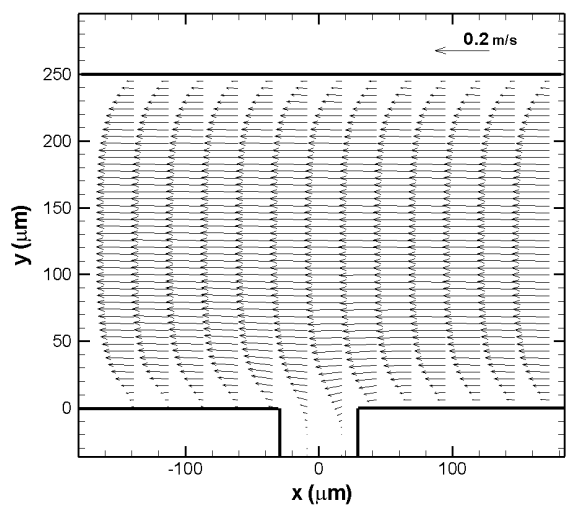

FIGURE 3. Velocity vectors in microchannel without jet flow

flow is from right to left, that is in the negative x direction. The

undisturbed profiles are typical velocity profiles for laminar flow in a rectangular duct. A comparison of the experimental velocity profiles with those obtained by the analytical solution [16] for steady flow in a rectangular duct is shown in Figure 4. The good agreement shown in Figure 4 validates the accuracy of the measurement technique and procedure used for setting the flow rate from the syringe pump. With the channel flow kept at constant

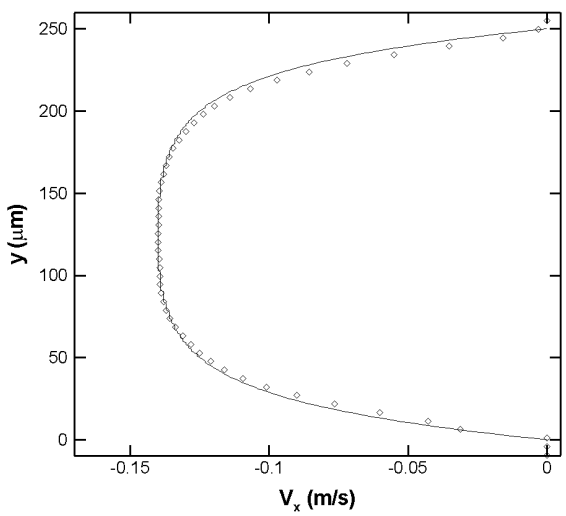

FIGURE 4. Comparison of experimental values of the *x*-velocity in microchannel (symbols) with the analytical solution for steady flow (solid line)

rate of 1.39μL/s, a sinusoidal signal with a peak to peak voltage of 35V and a frequency *f*, of 600Hz was supplied to the PZT disc. This frequency resulted is a Stokes number of 3. Velocity measurements were made at 18 different phases of the actuation cycle. The resultant, cross-flow, that is the *y*-velocity component distributions at the exit of the orifice are presented in Figures 5 and 6 for the ejection and ingestion phases of the cycle, respectively. From the velocity measurements it was not possible to determine when the diaphragm reached its zero velocity position at the end of the ingestion part of the cycle. This is also the time at which ejection phase begins and is usually used as the zero phase [1]. As a consequence, as may be seen in Figure 5, zero phase was defined as the first occasion after ingestion that all the velocity vectors in the orifice were in the positive *y*-direction. The non-dimensional time, $t^* = t/T$, in which t is the dimensional time and T is the period, was measured from this reference.

During the expulsion part of the cycle, with the exception of the results at zero phase, the profiles are well developed and

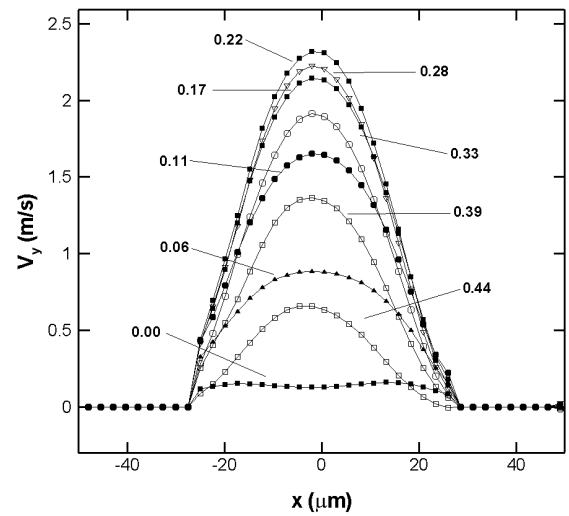

FIGURE 5. *y*-velocity profiles at orifice exit at various non-dimensional times during the ejection phase of the cycle

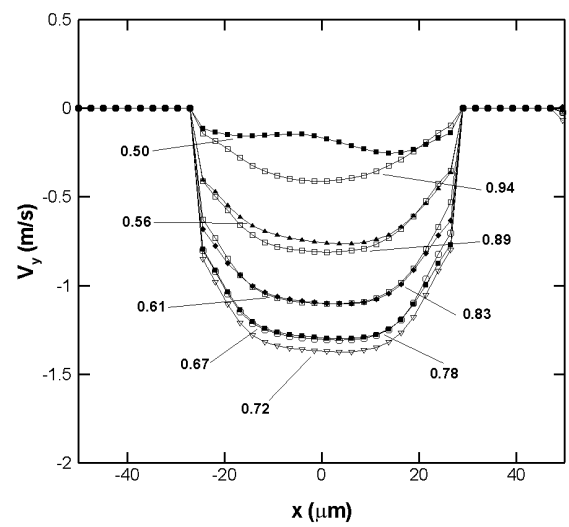

FIGURE 6. *y*-velocity profiles at orifice exit at various non-dimensional times during the ingestion phase of the cycle

are highly parabolic. The maximum velocity out of the orifice was 2.3m/s at t^*=0.22. Since the measurement were taken at the orifice outlet, that is in line with the lower surface of the microchannel shown in Figure 3, during ingestion, the velocity profiles shown in Figure 6 cannot develop. Hence, during ingestion, the velocity distribution was more uniform, perforce resulting in

lower peak velocities.

Velocity profiles on the centre plane at the exit of the orifice during the expulsion stage are compared in Figure 7 with those obtained analytically by Tsangaris and Vlachakis [17] for sinusoidally oscillating flow in a square duct at the same Stokes number. Since, as mentioned above, the velocity in the microchannel was from right to left (Figure 3), the experimentally obtained y-velocity distributions of the jet emanating from the orifice were displaced slightly to the left. Despite the effect of the flow in the channel, the experimental results are in surprisingly good agreement with the analytical solution.

The Reynolds number of the jet, Re_j, is an important parameter in determining its interaction with the main flow in the microchannel. It follows that the average velocity in space and time during ejection, needs to be determined. Since the velocity distribution was only known on the centre plane, it was not possible to evaluate from these values. The average velocity calculated from the analytic solution was 0.73m/s. This value was used as an estimate of $\overline{V_j}$. A jet Reynolds number of 43 resulted.

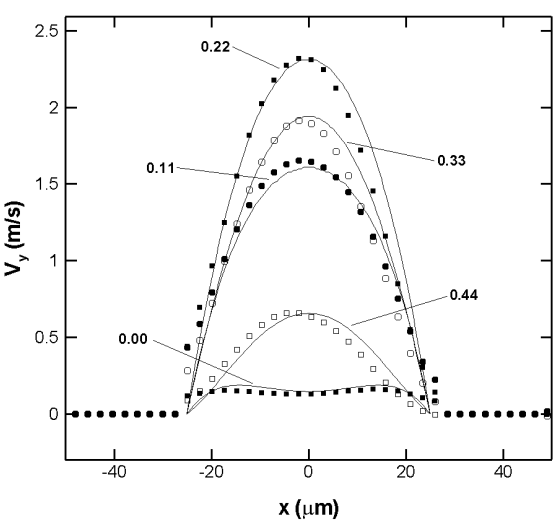

FIGURE 7. Comparison of the experimental values of the y-velocity at the exit of the orifice during ejection phase of the cycle (symbols) with the analytical solution for oscillatory flow (solid lines)

Synthetic jet flow fields

The ability of the synthetic jet to mix the flow in the main channel effectively, is demonstrated in the series of six instantaneous vectors plots in Figure 8. The vector plots are equally spaced in time across the actuation cycle. For clarity every 3rd vector is shown.

As may be seen in Figure 8(a), early in the ejection phase, t^*=0.11, the fluid expelled from the orifice forced the flow in the channel to divert around it. At t^*=0.28, Figure 8(b), just after the peak expulsion velocity had been reached, the increased velocity of the jet led to the flow separating at the edge of the orifice. This resulted in the formation of a pair of vortices on either side of the jet near the orifice. Here the jet has already impacted on the channel wall opposite the orifice. Since the fluid was supplied by the syringe pump at a constant rate, the fluid at least in the centre of the microchannel would need to have been forced towards the top and bottom of the channel. Measurements were attempted on planes other than the central plane, but were unsuccessful. As the jet velocity was reduced as may be seen in Figure 8(c) at t^*=0.44, the vortices had moved further towards the channel wall opposite the orifice, with the vortex on the left having almost reached it.

Even though the flow had reversed at t^*=0.61, Figure 8(d), the vortices continued to be transported towards the channel wall opposite the orifice with the vortex on the right now very close to that wall. During this time both vortices were convected downstream by the flow in the channel. The upstream vortex having impinged into the wall opposite the orifice, continued to lose its strength so that it cannot be seen on Figure 8(e) at t^*=0.78. From t^*=0.61 to t^*=0.78, Figure 8 (d) and (e), the downstream vortex lingers at x = -130μm and y = 150μm, gradually losing its strength until it can no longer be detected at t^*=0.94, Figure 8(f).

The behaviour of the jet during an actuator cycle shown in Figure 8, is similar to that found numerically in two-dimensional flow by Timchenko and her colleagues [7, 8]. In order to gauge the overall effect of the jet, the mean of the 18 phases was calculated and plotted in Figure 9. It is clearly seen that there are large differences between Figure 9 and Figure 3. Figure 9 shows that on the average there are two vortices on either side of a jet. These vortices are expected to significantly enhance mixing and heat transfer. Unfortunately, since at this stage only the velocity distribution on the centre plane was experimentally obtained, the mixing efficiency could not be evaluated. However, as mentioned above, Timchenko et al [6-8], whose numerical results are in excellent agreement with those presented here, have shown that a synthetic jet integrated in a microchannel significantly enhances heat transfer.

Timchenko and her colleagues had supposed in their numerical work on a synthetic jet integrated in a microchannel, [7, 8] that water was an incompressible fluid and the silicon wafer was a rigid solid. Since they had also assumed that a constant pressure difference was maintained between the ends of the microchannel, the flow rate in that channel could vary throughout an actuator cycle. However, in the present work the syringe pump supplied a constant flow rate. When the synthetic jet was switched on water flowed into the chamber of the synthetic jet generator for part of the cycle and out of that chamber for the

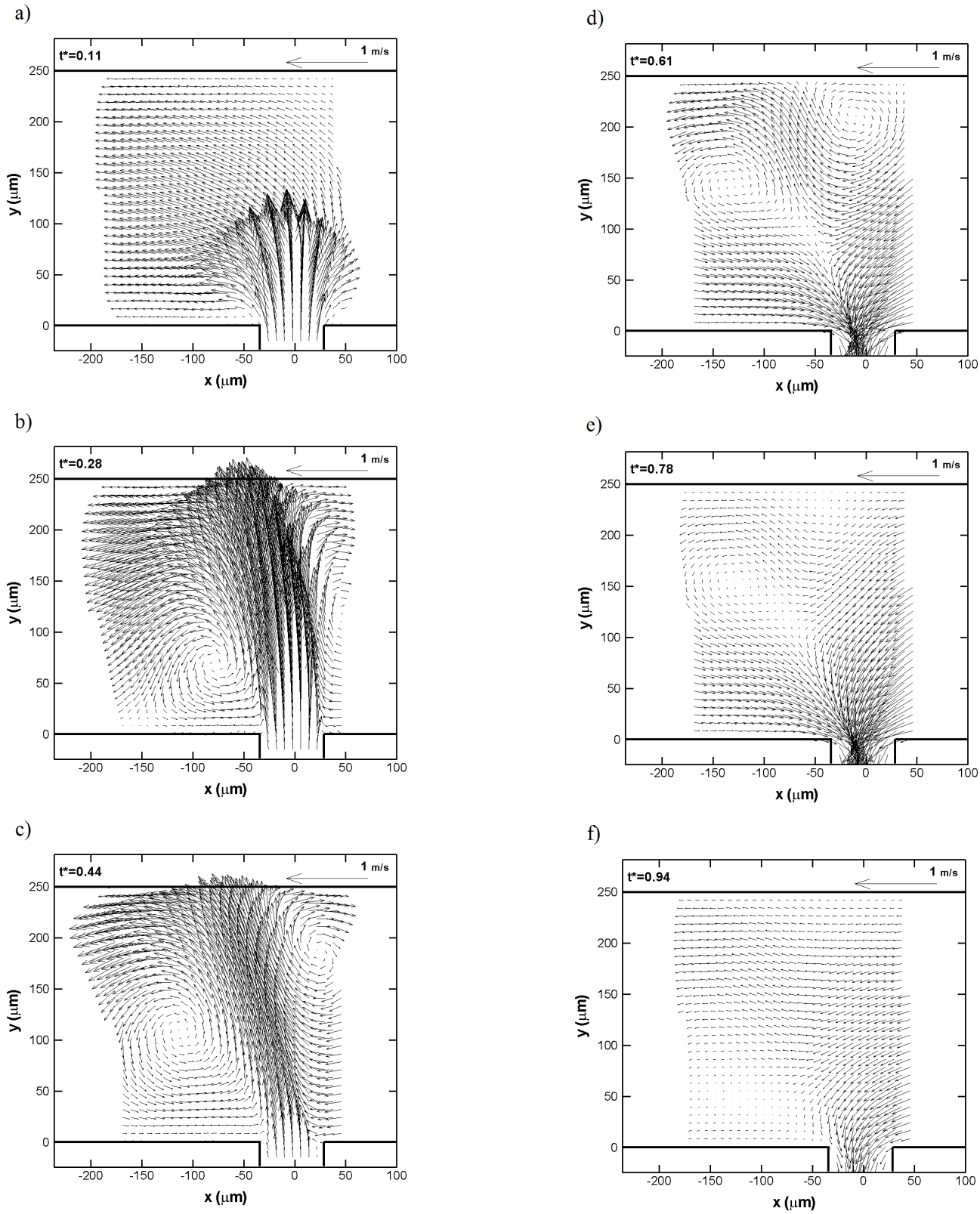

FIGURE 8. Sequence of velocity vectors at various phases throughout the actuation cycle in the vicinity of the orifice

remainder of the cycle. As may be seen in Figures 8 and 9 these flows severely disrupted the fluid stream in the microchannel. Since at the low pressures involved in the present experiments, for all practical purposes, water could be considered to be incompressible and the structure of the apparatus rigid, the question then arose: was the flow rate in the microchannel constant throughout the synthetic generator cycle?

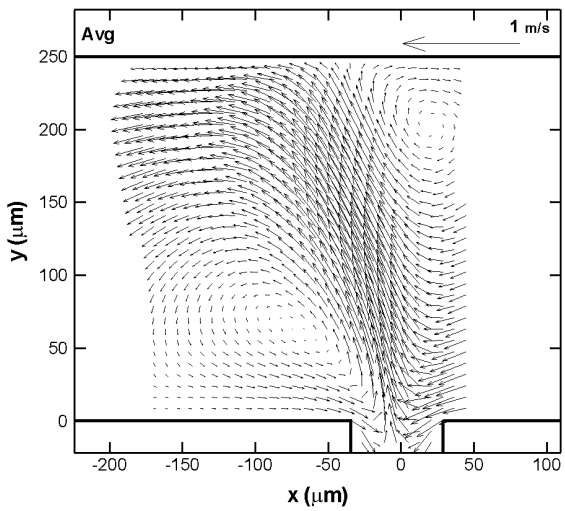

FIGURE 9. Mean velocity field in the vicinity of the orifice

The beaker in Figure 2 into which the fluid issued from the microchannel was placed on an accurate balance, so that the time taken for a given mass of fluid to flow into it could be determined with an accurate stopwatch. The flow rate could then be determined. It was shown to within 1% that, at least on the average, the flow rate had been correctly set at 1.39μL/s.

While the flow rate downstream of the orifice would necessarily vary during an actuation cycle, since the syringe pump delivered a constant flow rate of 1.39μL/s at its outlet the flow upstream of the orifice could not have varied if the walls of the apparatus had been rigid and the fluid used incompressible. However, as may be seen in Figure 10 the flow approximately 1mm upstream of the orifice is far from steady. The line with the solid symbols in Figure 10 is the velocity profile from Figure 3 and 4 when there was no jet actuation and represents the expected profile for a forced flow rate in a system in which all the boundaries are rigid and the fluid is incompressible.

During the ejection part of the cycle (phases 0 to 0.50) the flow rate in the microchannel was in general lower than the steady value. In fact, once the channel had completely become blocked by the synthetic jet between $0.28 \leq t^* \leq 0.39$ there was a reversal of flow in the channel despite, as already mentioned a number times, that the syringe pump supplied a constant flow rate. During suction, as may also be seen in Figure 10 the reverse was found in that the velocities were equal to or greater than the steady values. Thus, while the average flow rate was inevitably the flow rate supplied by the syringe pump, the instantaneous value was quite different. The difference between the

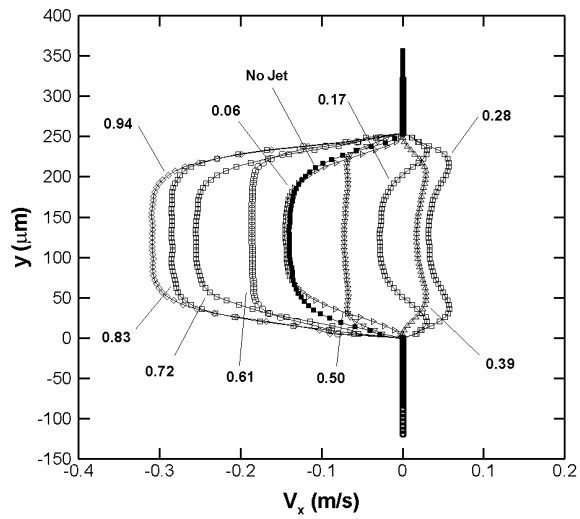

FIGURE 10. x-velocity distributions in the microchannel at various times of the actuator cycle, approximately 1mm upstream of the orifice

instantaneous velocity distributions upstream of the orifice and the steady flow values could only be explained by there being a means of storing liquid between the syringe pump outlet and the position at which the velocities were measured. It follows that there were trapped air bubbles, or that the connecting tubing provide the necessary compliance, or a combination of both effects. A thorough inspection of the microchannel failed to reveal any trapped bubbles of air or sufficient compliance in the tubing. This illustrates one of the great difficulties of working at the microscale; the ability to fully fill microdevices with liquid remains an unsolved problem.

CONCLUSION

A synthetic microjet integrated in a microchannel was successfully designed and fabricated using traditional micromachining techniques.

MicroPIV measurements in the vicinity of the orifice were performed, phase locked to the actuation signal of the synthetic

microjet generator. At a peak to peak voltage of 35V and a frequency f=600Hz a maximum velocity of 2.3m/s was achieved. The profiles at the exit of the orifice were highly parabolic during expulsion and were in good agreement with the analytical solution for oscillatory flow in a square duct.

The phase locked velocity vector patterns showed that during the ejection part of the cycle a jet was formed at the orifice that had sufficient strength to impinge on the channel opposite the orifice. The pair of vortices formed at the edge of the orifice traveled away from it with the jet. The vortices lost their strength and were no longer detectable by the end of the ingestion phase of the cycle.

Finally, it was found that the flow patterns presented in this study were affected by a compliance source upstream of the orifice. This effect will be examined in more detail in future work.

ACKNOWLEDGMENT

The authors gratefully acknowledge the financial support of the Australian Research Council through grant DP0667136. The authors would also like to thank Hemant Bhatta, Aaron Michael from UNSW and Arnan Mitchell RMIT for their help with different aspects of the fabrication.

REFERENCES

[1] Smith, B. L. and Glezer, A., 1998, 'The formation and evolution of synthetic jets', *Physics of Fluids*, Vol. 10, pp. 2281-2297

[2] Campbell, J. S., Black, W. Z., Glezer, A. and Hartley, J. G., 1998, 'Thermal management of a laptop computer with synthetic air microjets', *Seattle, WA: ITherm98, Sixth Intersociety Conference on Thermal and Thermomechanical Phenomenon in Electronic Systems*, pp. 43-50

[3] Chen, Y., Liang, S., Aung, K., Glezer, A. and Jagoda, J., 1999, 'Enhanced mixing in a simulated combustor using synthetic jet actuators', *Reno, NC: AIAA Paper 1999-0449*

[4] Amitay, M., Kibens, V., Park, D. and Glezer, A., 1999, 'The dynamics of flow reattachment over a thick airfoil controlled by synthetic jet actuators', *Reno, NV: AIAA Paper 1999-1001*

[5] Timchenko, V., Reizes, J. and Leonardi, E., 2007, 'An Evaluation of Synthetic Jets for Heat Transfer Enhancement in Air Cooled Micro-channels', *Int. J. Numerical methods for Heat and Fluid Flow*, Vol. 17, No. 3

[6] Li, D., Timchenko, V., Reizes, J. A., and Leonardi, E., 2007, 'The Effect of Frequency and Wave Shape Generated by a Synthetic Jet Actuation on the Cooling of Microchips With Channels Filled With Water', *16th Australasian Fluid Mechanics Conference, Crown Plaza, Gold Coast, Australia, 2-7 December 2007*

[7] Timchenko, V., Reizes, J., Leonardi, E., and Stella, F., 2005, 'Heat Transfer Enhancement using Synthetic Jet Actuators in Forced Convection Water Filled Micro-Channels' *Proceedings of the 3rd IASME/WSEAS Int. Conf. on HEAT TRANSFER, THERMAL ENGINEERING AND ENVIRONMENT, Corfu, Greece, August 20-22, 2005*, pp.294-299

[8] Maunter, T., 2004, 'Application of the synthetic jet concept to low Reynolds number biosensor microfluidic flows for enhanced mixing: a numerical study using the lattice Boltzmann method', *Biosensors and Bioelectronics*, Vol. 19, pp. 1409-1419

[9] Liu, M., Xie, C., Zhang, X., and Chen, Y., 2008, 'Numerical simulation on micromixer based synthetic jet', *Acta Mech Sin*, Vol. 24, pp. 629-636

[10] Mallinson, S. G., Kwok, C. Y. and Reizes, J. A., 2003, 'Numerical simulation of micro-fabricated zero mass-flux jet actuators', *Sensors and Actuators A*, Vol. 105, pp. 229-236

[11] Guo, F. and Zhong, S., 2006, 'A PIV Investigation of the Characteristics of Micro-scale Synthetic Jets', *3rd AIAA Flow Control Conference 5-8 June 2006, San Francisco, California, USA, AIAA paper 2006-3183*

[12] Sinclair, A., Timchenko, V., Reizes, J., Rosengarten, G., and Leonardi, E., 2008, 'An experimental and numerical study of a micro-synthetic jet in a shallow cavity', *6th ASME conference on Nanochannels, Microchannels, and Minichannels, Darmstadt Germany*

[13] Morris, C. J., and Forster, F. K., 2003, 'Low-Order Modeling of Resonance for Fixed-Valve Micropumps Based on First Principles', *J. Microelectromechanical Systems*, Vol. 12, pp. 325-334

[14] Meinhart, C. D., Wereley, S. T. and Santiago, J. G. 1999, 'PIV measurements of a microchannel flow', *Experiments in Fluids*, Vol. 27, pp. 414-419

[15] Olsen, M. G. and Adrian, R. J., 2000, 'Out-of-focus effects on particle image visibility and correlation in microscopic particle velocimetry', *Experiments in Fluids*, Vol. 29, pp. S116-S174

[16] White, F. M., 2006, 'Viscous Fluid Flow', Third Edition, McGraw-Hill International Edition

[17] Tsangaris, S., and Vlachakis, N. W., 'Exact Solution of the Navier-Stokes Equations for the Fully Developed, Pulsating Flow in a Rectangular Duct With a Constant Cross-Sectional Velocity', *Journal of Fluids Engineering*, Vol. 125, pp. 382-385